On the Relation between NDVI, Fractional Vegetation Cover, and Leaf Area Index

Article *in* Remote Sensing of Environment · December 1997

DOI: 10.1016/S0034-4257(97)00104-1

2 authors, including:

Toby Carlson
Pennsylvania State University
146 PUBLICATIONS **15,644** CITATIONS

ELSEVIER

On the Relation between NDVI, Fractional Vegetation Cover, and Leaf Area Index

Toby N. Carlson and David A. Ripley**

We use a simple radiative transfer model with vegetation, soil, and atmospheric components to illustrate how the normalized difference vegetation index (NDVI), leaf area index (LAI), and fractional vegetation cover are dependent. In particular, we suggest that LAI and fractional vegetation cover may not be independent quantitites, at least when the former is defined without regard to the presence of bare patches between plants, and that the customary variation of LAI with NDVI can be explained as resulting from a variation in fractional vegetation cover. The following points are made: i) Fractional vegetation cover and LAI are not entirely independent quantities, depending on how LAI is defined. Care must be taken in using LAI and fractional vegetation cover independently in a model because the former may partially take account of the latter; ii) A scaled NDVI taken between the limits of minimum (bare soil) and maximum fractional vegetation cover is insenstive to atmospheric correction for both clear and hazy conditions, at least for viewing angles less than about 20 degrees from nadir; iii) A simple relation between scaled NDVI and fractional vegetation cover, previously described in the literature, is further confirmed by the simulations; iv) The sensitive dependence of LAI on NDVI when the former is below a value of about 2–4 may be viewed as being due to the variation in the bare soil component. ©*Elsevier Science Inc., 1997*

BACKGROUND

The normalized difference vegetation index (NDVI) is defined as

$$NDVI=\frac{(a_{nir}-a_{vis})}{(a_{nir}+a_{vis})}, \quad (1)$$

where a_{nir} and a_{vis} represent surface reflectances averaged over ranges of wavelengths in the visible ($\lambda\sim0.6$ μm, "red") and near infrared, IR ($\lambda\sim0.8$ μm) regions of the spectrum, respectively. It is clear from its definition that the NDVI (like most other remotely sensed vegetation indices) is not an intrinsic physical quantity, although it is indeed correlated with certain physical properties of the vegetation canopy: leaf area index (LAI), fractional vegetation cover, vegetation condition, and biomass. As such, vegetation indices are highly useful measurements despite their limitations.

The NDVI has been criticized because of the following perceived defects:

1. Differences between the "true" NDVI, as would be measured at the surface, and that actually determined from space are sensitive to attenuation by the atmospheric and by aerosols.
2. The sensitivity of NDVI to LAI becomes increasingly weak with increasing LAI beyond a threshold value, which is typically between 2 and 3.
3. Variations in soil brightness may produce large variations in NDVI from one image to the next (Liu and Huete, 1995).

Accordingly, various investigators have addressed these problems in light of indices that exhibit a better correlation with leaf area and less sensitivity to soil brightness changes or to atmospheric attenuation than does NDVI (Jasinski, 1996; Leprieur et al., 1996; Liu and Huete, 1995; Pinty and Verstraete, 1992).

That the relation between NDVI and LAI undergoes a marked decrease in sensitivity above a loosely defined threshold is well known from measurements. Carlson et al. (1990) stated that

NDVI increases almost linearly with increasing LAI

* Department of Meteorology, The Pennsylvania State University, University Park

Address correspondence to Dr. Toby N. Carlson, Dept. of Meterology, The Pennsylvania State University, University Park, PA 16802.

Received 23 December 1996; revised 6 June 1997.

REMOTE SENS. ENVIRON. 62:241–252 (1997)

655 Avenue of the Americas, New York, NY 10010

0034-4257/97/$17.00
PII S0034-4257(97)00104-1

and then enters an asymptotic regime in which NDVI increases very slowly with increasing LAI. Curran (1983) points out that the latter asymptotic region pertains to a surface almost completely covered by leaves. Although there is some variation, the upper asymptote of NDVI versus vegetation density or LAI usually occurs near 0.5–0.8 for dense vegetation. This upper limit, however, is rather variable and depends on vegetation type, age, and leaf water content (Paltridge and Barber, 1988). For bare soil NDVI tends to vary between −0.1 and 0.2.

Curran also shows that the asymptotic region for LAI begins at values of 3–4 for short crops such as wheat, corn sorghum, and various grasses. Asymptotic regimes for LAI were found by Tucker (1979), Holben et al. (1980) for soybeans (above 2), Asrar et al. (1984) for wheat (above 2.5), Best and Harlan (1985) for oats (above 2), Gallo et al. (1985) for corn (above 3) and Sellers (1985) for various idealized canopies (above values from 1 to 3, depending on leaf angle). Nemani and Running (1989) show that the change in LAI is nearly linear with NDVI until the former exceeds values of 3–4, above which NDVI rapidly approaches an asymptotic limit.

Admittedly, the threshold value must be arbitrarily defined, but it is apparent that, beyond a certain value of LAI, the change in NDVI with LAI becomes insignificant. Aside from the references cited in the preceding excerpt, Price (1992), Liu and Huete (1995), and Jasinski (1996) have more recently shown that this threshold tends to be reached when LAI attains a value between 2 and 3. The decrease in sensitivity of NDVI to changing LAI at higher values of the latter occurs because the reflectance of solar radiation from the underlying soil surface or lower leaf stories is largely attenuated when the ground surface is completely obscured by the leaves. Although this property of NDVI is undoubtedly a deficiency for some applications, such as inferring total biomass, it can also be advantageous in identifying the value of NDVI for which surfaces are just reaching 100% vegetation cover, above which NDVI is almost insensitive to changing vegetation amount. The importance of this threshold value of NDVI between being sensitively dependent on LAI and the asymptotic regime will be made clear in the Results section.

Our perception of how LAI relates to fractional vegetation cover requires further clarification. LAI is customarily defined as the total one-sided leaf-surface area measured over a unit horizontal ground-surface area (e.g., 1 m^2). Fractional vegetation cover pertains to the part of a vegetation canopy having no patches of bare soil between plants, although small holes in the vegetation cover and sun flecks at the surface are permissible. It is reasonable to suppose from observations that an LAI of less than 1.0 would tend to involve a fractional vegetation cover of less than 100%. In practice, however, LAI values of less than about 2–4 are likely to exhibit some bare soil surfaces.

Consider a situation in which the canopy contains openings between plants, through which some bare soil is visible. These openings may correspond to spaces between plants, to rows, or to open spaces. It follows that LAI measured where no breaks in the canopy are visible would generally exceed the LAI measured without regard to the presence of breaks in the canopy. In fact, the former, a *local* LAI, would always equal or exceed the latter, the *global* LAI. The differences between global and local LAI would be considerable if the domain included only a few small plants.

Local versus global LAI may appear at first to be an unnecessary distinction, because only the latter is reported in the literature, but the difference is critical for understanding the relevance to LAI in SVAT (soil-vegetation-atmosphere-transfer) models. Virtually all land-surface components operating today for example, BATS (Dickinson et al., 1993), SiB (Sellers and Dorman, 1987) LSX (Pollard and Thompson, 1995), PLACE (Wetzel and Boone, 1995), and PSUBAMS (Gillies et al., 1997) make use of the so-called big leaf assumption alluded to by Monteith (1973), in which the canopy resistance corresponds to an equivalent leaf resistance. This leaf stretches across a surface domain of indeterminate size represented by a one-dimensional column model containing layers of soil, vegetation, and atmosphere. Although multiple leaf stories may be prescribed with vegetated and nonvegetated surfaces treated in parallel, the big leaf assumption strictly represents a surface uniformly and completely covered by vegetation. A small value of LAI pertaining to a field with bare patches is therefore incompatible with the big leaf. That big leaf models tend to work satisfactorily in spite of such contradictions does not necessarily ensure that they are realistic in their dependence on LAI. In principle, big leaf models should apply to areas where the local LAI is an appropriate measure.

It seems plausible that the variation of NDVI with respect to the global LAI in partially vegetated areas—that is, in regions where the global LAI is below a rather imprecisely defined threshold of 2–4—could be explained largely by the variation in the fraction of nonvegetated surface area illuminated by the sun and visible to the radiometer. (Here, we ignore the effects of shading, which further complicate the picture.) An independent specification of a global LAI may therefore be redundant or incompatible with the specification of fractional vegetation cover in regions of partial vegetation cover.

The purpose of this paper is to present some simple radiative transfer calculations that show:

1. the variation of NDVI with local and global LAI;
2. that the customary variation of NDVI with LAI

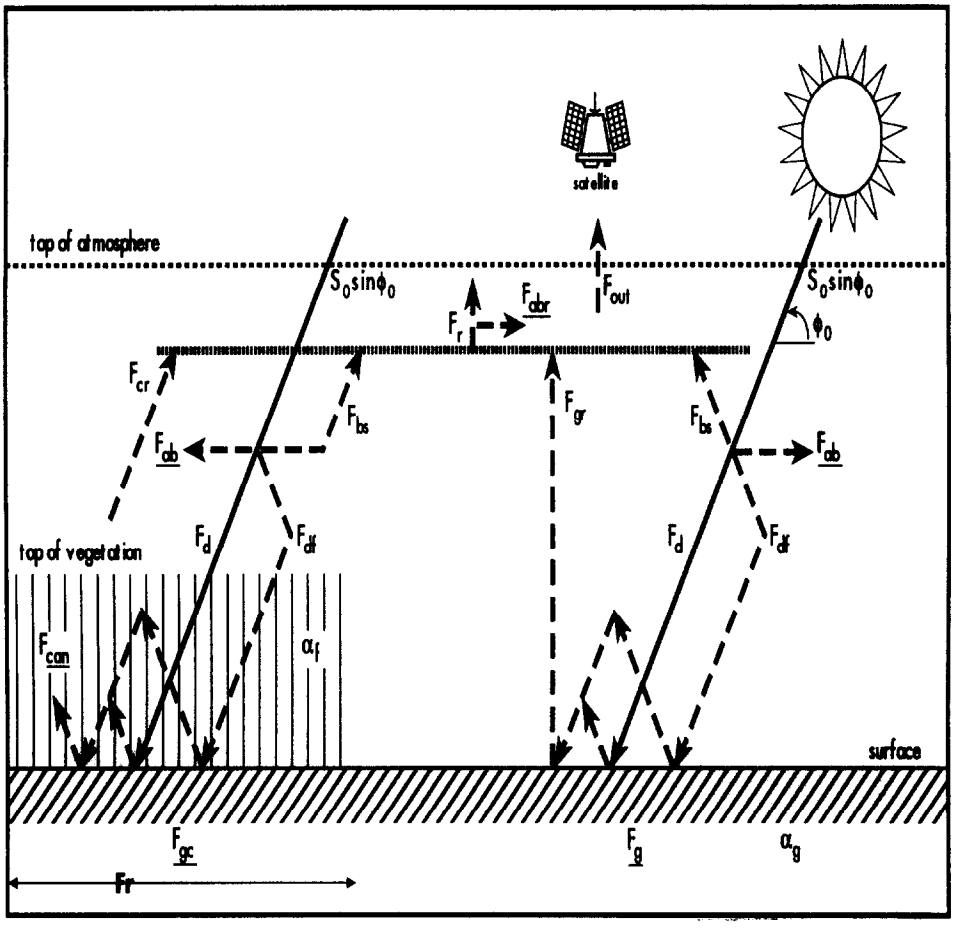

Figure 1. Schematic representation of radiative flux components in the simple model. Solid lines with arrows represent the direct solar flux component at elevation angle φ_0, dashed lines represent diffuse flux components over a bare soil fraction (right side) and a vegetated fraction (*Fr*; left side). Fluxes are represented by the symbol *F* with subscripts denoting various flux components either absorbed in the atmosphere, absorbed at the ground or within the vegetation canopy, scattered upward or downward, or reflected upward. (All absorbed fluxes are underlined.) The flux to space measured by a satellite radiometer is indicated by the dashed line labeled F_{out} (see Appendix).

can be largely explained by a variation in fractional vegetation cover;

3. that NDVI decreases much less rapidly with increasing global LAI when the fractional vegetation cover reaches 100%;
4. that scaling the NDVI between values for bare soil and for 100% vegetation cover factors out most of the atmospheric correction; and
5. further evidence to confirm the existence of a simple relation between scaled NDVI and fractional vegetation cover.

THE MODEL

The radiative transfer model, described in the Appendix, is a very simple two-stream (upward and downward) representation of fluxes through a one-layer atmosphere over a surface consisting of bare soil and a single layer of vegetation. The latter is represented by an unbroken vegetation canopy (represented by a local LAI) occupying a fraction, *Fr*, of the total domain whose global LAI is equal to *Fr* times the local LAI.

Figure 1 illustrates the various flux streams that undergo absorption, scattering, and reflection as they move through the atmosphere and the vegetation layer. Scattering and reflection are either upward or downward. Reflectances and their derivative product, NDVI, are determined at the surface and at the top of the atmosphere.

NDVI is derived from reflectance values that are calculated separately in two wavelength bands in the visible (0.5–0.7 μm) and near infrared (0.7–0.9 μm) regions of the spectrum. The radiation scheme is as follows. A beam of direct solar radiation at solar elevation angle φ_0 is incident at the top of the atmosphere. Some of that incident flux in the downward direct beam is absorbed by the atmosphere (F_{ab}), a part is scattered upward as diffuse flux (F_{bs}), and another component is scattered downward as diffuse flux(F_{df}), which, along with the unattenuated direct flux, is incident on the ground and the top of the vegetation canopy. The combined diffuse and direct flux incident at the ground, whose albedo is α_g, is divided between a component absorbed at the ground in the bare soil area (F_g) and a component reflected upward (F_{gr}).

An identical incident flux is absorbed by the vegetation canopy (F_{can}) and by the ground underneath the vegetation canopy (F_{gc}). The remaining flux, that not absorbed in the vegetation and at the ground, is reflected upward (F_{cr}). Upward flux streams reflected from the atmosphere, the bare soil, and the vegetation canopy (and its underlying soil) combine to form the total upward flux

(F_r). The total upward flux is further attenuated by absorption, which removes an amount of flux (F_{abr}). No account is taken of backward scattering of this upward radiation stream.

The flux reaching the satellite is determined indirectly by subtracting all absorbed atmosphere and surface components from the incident flux at the top of the atmosphere. The apparent reflectance is calculated by dividing the upward flux at the top of the atmosphere (F_{out}) by the exoatmospheric solar flux [Eq. (A10)]. Surface reflectance is determined as a ratio of the sum of reflected fluxes at the surface divided by the incident surface flux [Eq. (A8)]. Satellite angle is considered only insofar as it affects the path length of the reflected flux component F_r toward the satellite. NDVI is calculated, by Eq. (1).

Model initialization requires specifying the reflectances for bare soil and leaves, the fractional vegetation cover, time of day, satellite viewing angle, local LAI, latitude, longitude, horizontal visibility (from which aerosol optical depth is calculated), and a few other variables of much less importance, such as surface pressure and ozone concentration (see Table A1).

As presented in the Appendix, the radiative transfer formulation does not constitute a rigorous treatment of the radiation physics; nor is the treatment particularly new. The purpose of the radiation model is to provide a reasonable estimate of the major radiation components in the atmosphere, in a vegetation layer, and at a bare soil surface. Our confidence in the model's efficacy is based on its long-term satisfactory performance as a solar radiation component within a SVAT model (Gillies et al., 1997). Direct (unpublished) comparisons of simulated and measured solar fluxes have been made, and these comparisons show agreement within about 5%. More important, however, the SVAT model has been widely employed in conjunction with remote and in situ measurements to investigate land-surface processes, particularly the role of soil moisture in modifying the surface-energy budget (Gillies et al., 1997), the determination of transpiration fluxes over plants, and the intake of carbon in plant canopies (Olioso et al., 1996). Further validation by comparison with another model is presented in the next section.

RESULTS

Initial Conditions

Radiative transfer simulations were made for the latitude and longitude of State College, PA (approximately 40° N and 76° W), for a July day over a range of times from noon until 2:00 P.M. and satellite zenith angles from 0 to 20 degrees from nadir. Because results were similar for all satellite and sun angles investigated, all illustrations refer to one time and one viewing angle—1:00 P.M. local time 20 degrees from nadir.

Table 1. Albedos of Bare Soil and Leaves (%)

	Visible	*Near IR*
Soil	8	11
Leaves	5	50

Fractional vegetation cover (*Fr*) was varied from 0.0 to 1.0, the local LAI remaining fixed. Global LAI, equal to *Fr* times the local LAI, is not directly used in the calculations, but this parameter is referred to in the illustrations. For example, a local LAI of 3 and a value of *Fr* equal to 50% corresponds to a global LAI of 1.5. At *Fr*=100%, global and local LAI are identical. Values of the local LAI for an *Fr* value of less than 1.0 were fixed at a value of 3.0 in most simulations, but a few simulations were made by using a local LAI of 2.0 and of 4.0. Additional simulations were made at *Fr*=1, by varying LAI in increments from the local LAI for the partial cover case to LAI=10. All calculations refer to clear sky conditions.

Albedos pertaining to the bare soil surface (a_g, including the albedo beneath the canopy) and to the leaves (a_f) were fixed for all simulations; they are identical for diffuse and direct flux. Table 1 refers to these fixed reflectances, thereby fixing NDVI for bare soil and at the limiting values in the asymptotic regime (infinite LAI). The purpose in choosing this particular combination of albedos is that they yield the range of NDVI typically measured by satellite over a mixture of bare soil and vegetation (Gillies and Carlson, 1995). (The values are not meant to be representative of any particular soil or vegetation types.)

To simulate normal and hazy conditions, two differing visibility values were used: 15 and 5 km. They were converted into aerosol optical depth, as indicated in the Appendix. A summary of parameters used to perform the simulations and selected values of reflectance obtained thereof are presented in the Appendix in Table A1.

Comparisons with MODTRAN

MODTRAN (Kneizys et al., 1996), a more recent version of LOWTRAN (Kneizys, 1988), is considered a standard model for making atmospheric correction to satellite radiance measurements. As such, it is normally employed to correct all our satellite and aircraft images for atmospheric attenuation for both the solar and the thermal IR part of the spectrum (Gillies et al., 1997). MODTRAN does not account for vegetation, but it does require a temperature and humidity sounding and an estimate of horizontal visibility.

A comparison between NDVI simulated with the simple model described in the Appendix and MODTRAN was made as follows. Tables of surface and apparent (at sensor) reflectances were generated by using both the simple model and MODTRAN and were subse-

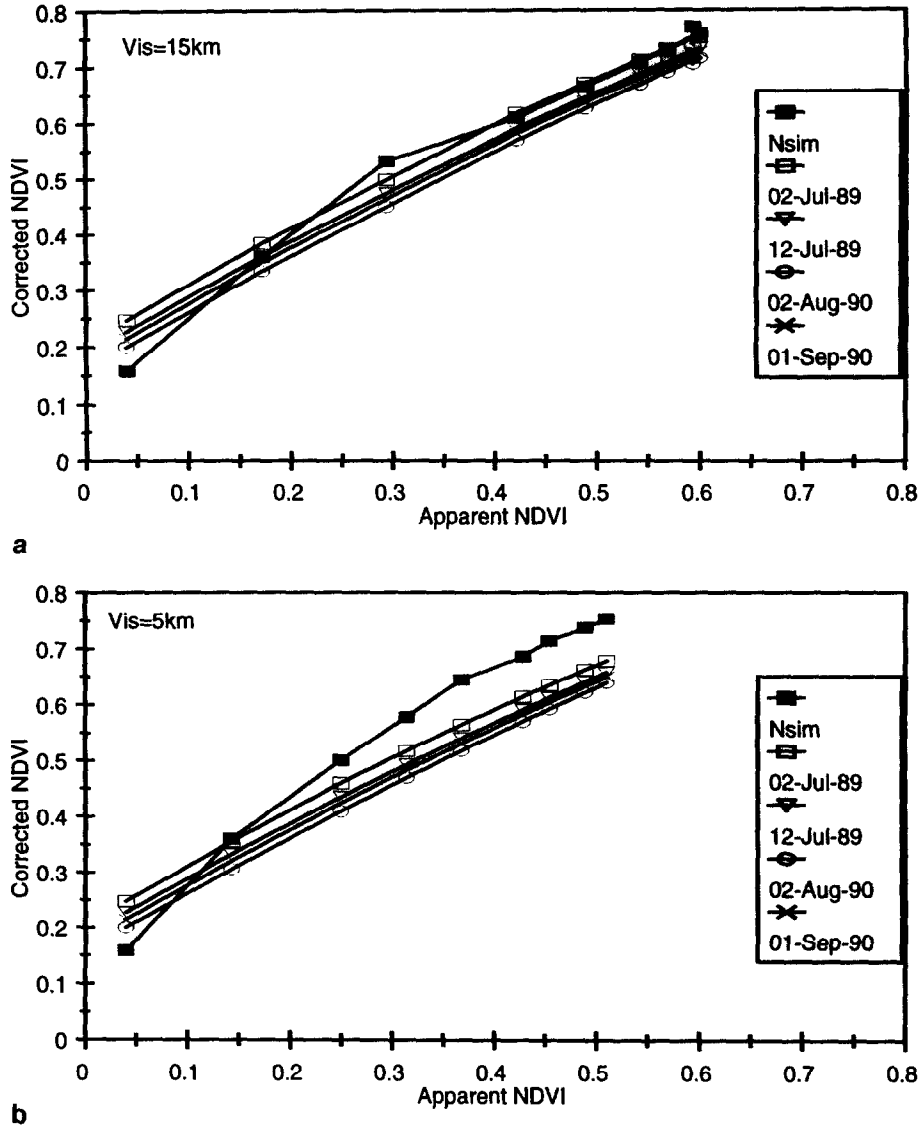

Figure 2. NDVI converted into at-surface values for atmospheric attenuation by using MODTRAN for four atmospheric temperature and moisture soundings made over Pennsylvania on differing days (see key) and the corrected NDVI based on the radiative transfer model simulations (Nsim) described in the text (solid rectangles) versus the uncorrected (apparent) NDVI for values used in the simulations: (a) 15-km visibility; (b) 5-km visibility.

quently used to calculate corresponding values of surface and apparent NDVI. In this manner, a set of values of corrected and uncorrected or apparent NDVI were made for both models over a range of values of fractional vegetation cover and LAI. Four different sets of initial temperature and moisture soundings were used for the MODTRAN calculations.

Figure 2 shows the results of the comparison of the corrected (at-surface) NDVI and the apparent (at-satellite) NDVI for normal and hazy conditions (visibility=15 km and 5 km, respectively). The relation is nearly linear for both models, and the results are very similar, although agreement was not quite as good for the hazy conditions. As in Pinty and Verstraete (1992), the corrected NDVI is approximately 0.15–0.2 greater than the apparent (measured) NDVI.

NDVI as a Function of LAI

Local LAI was set at a fixed value of 3, and the fractional vegetation cover was varied from 0 to 1. In the asymptotic regime ($Fr=1$), LAI was increased incrementally from 3 to 10. Figure 3a (15-km visibility) shows that the apparent NDVI increases from 0.54 to 0.61 and the corrected NDVI from 0.72 to 0.75 as LAI increases from the 100% vegetation cover threshold to LAI=10 in the asymptotic regime. Figure 3b is similar but shows a lower NDVI in the asymptotic regime for this hazy case (visibility=5 km).

Additional simulations for the 15-km visibility case were made for a local (threshold) LAI of 2 and of 4 (Fig. 4). These simulations show an increase of apparent NDVI from 0.47 to 0.60 and the corrected NDVI from 0.57 to 0.76 in the asymptotic regime (LAI greater than 2). For a threshold LAI of 4, the increase in NDVI in the asymptotic regime (LAI between 4 and 10) was from 0.57 to 0.60 for the apparent NDVI and from 0.74 to 0.76 for the corrected NDVI. Little change occurred in any of the simulations for a LAI greater than about 6.

Because the most likely values of local LAI for vegetated surface just reaching 100% cover are between 2

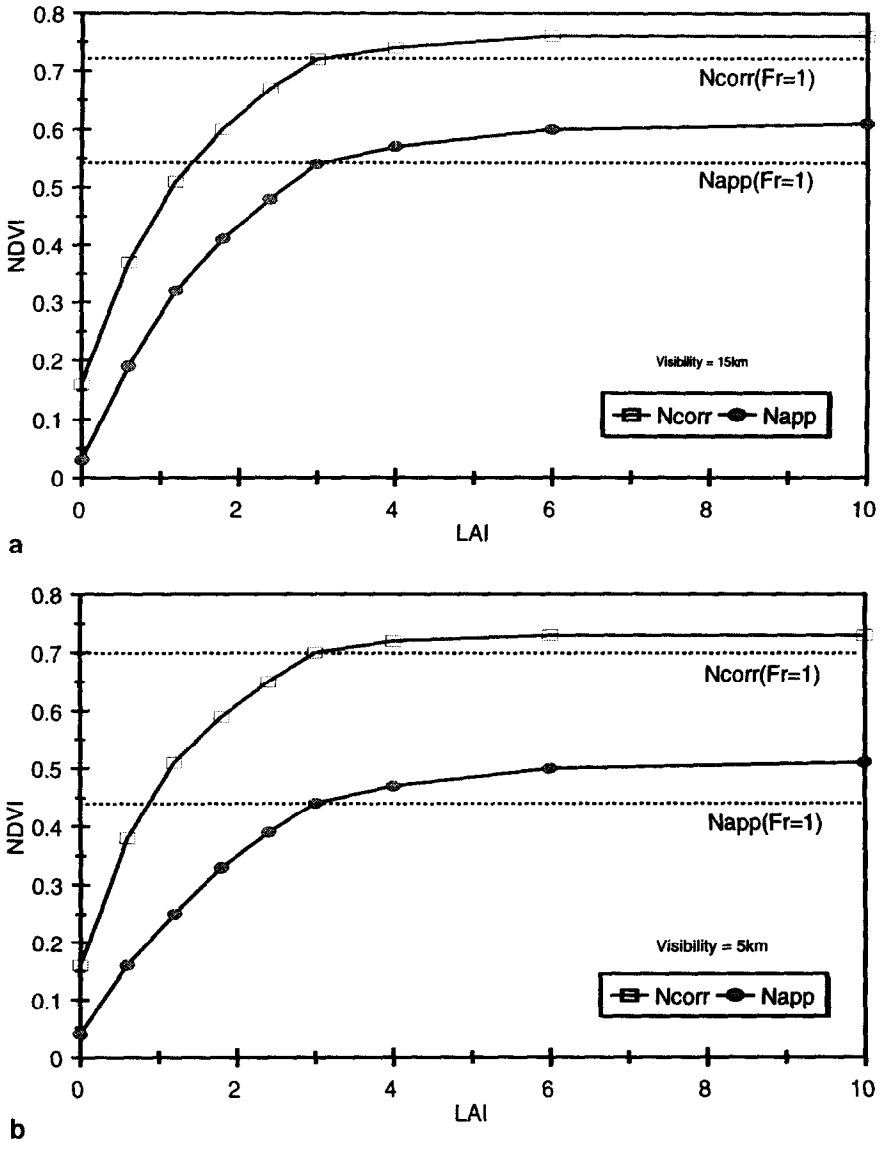

Figure 3. Uncorrected (apparent; Napp) NDVI and NDVI corrected to surface values (Ncorr) versus global LAI; [global LAI is equal to the fractional vegetation cover (*Fr*) times a fixed value of local LAI of 3 up to 100% vegetation cover, above which local and global LAI are equal]: (a) for 15-km visibility; (b) for a 5-km visibility. Horizontal dotted lines denote the value of NDVI at the threshold to the asymptotic regime in which fractional vegetation cover is just reaching 100% (*Fr*=1).

and 4, we can infer from Figures 3 and 4 that the apparent NDVI at the asymptotic threshold is likely to be between 0.05 and 0.10 below the values pertaining to an infinitely large LAI. It seems reasonable to suppose, therefore, that the NDVI for areas in which the vegetation cover is just reaching 100% will be adequately represented by values slightly less than the maximum found in the image over dense vegetation.

Scaling the NDVI

The advantage of a scaled NDVI in minimizing uncertainty in the initial conditions in models that yield soil water content and surface energy fluxes by inversion of a SVAT model has been pointed out by Gillies et al. (1997). An added benefit in scaling NDVI can now be seen. Scaled NDVI (N^*) is defined as

$$N^* = \frac{NDVI - NDVI_0}{NDVI_s - NDVI_0}, \tag{2}$$

where $NDVI_0$ and $NDVI_s$ correspond to the values of NDVI for bare soil (LAI=0) and a surface with a fractional vegetation cover of 100%, respectively.

Using entirely different approaches and data sources from this paper, Choudhury et al. (1994) and Gillies and Carlson (1995) independently obtained an identical square root relation between N^* and Fr, which is stated:

$$Fr \approx N^{*2}. \tag{3}$$

Figure 5 shows N^{*2} versus Fr for both the corrected and uncorrected NDVI values for the 15-km visibility and 5-km visibility cases. Figure 6 is identical in form with Figure 5a but for the other two threshold values (2 and 4) of LAI, both corrected and uncorrected. In all cases, the curves conform closely to Eq. (3), with the maximum deviation in Fr being generally less than 0.1. An important implication here is that atmospheric correction of the scaled NDVI is unnecessary for determining fractional vegetarian cover and LAI, because N^* [and there-

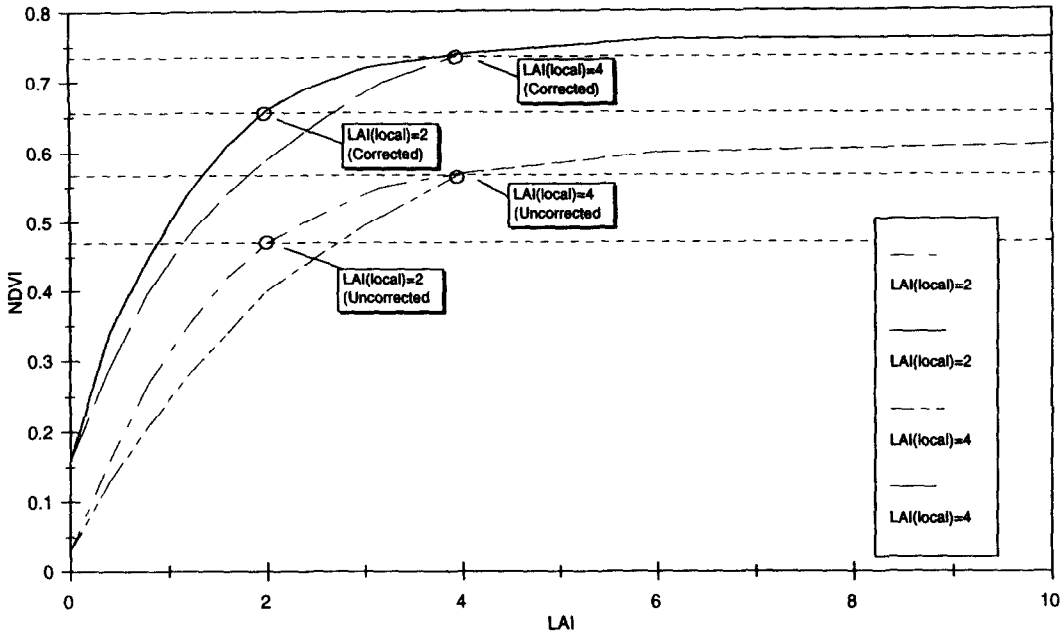

Figure 4. Same as Figure 3a (15-km visibility) but for differing LAI thresholds of 2 and 4, corrected and uncorrected radiances.

fore Eq. (3)] is approximately the same for both corrected and uncorrected NDVI. That the atmospheric correction effectively cancels in making the scaling from NDVI to N^* is a consequence of the linearity between corrected and uncorrected NDVI, as indicated in Figure 2.

CONCLUSIONS

We show with the aid of a simple radiative transfer model that the characteristic behavior of NDVI as a function of LAI can be simulated by changing only fractional vegetation cover when it is less than 100%. NDVI is sensitive to changes in the fractional vegetation cover until a full cover is reached, beyond which a further increase in LAI results in an additional small and asymptotic increase in NDVI. The change in regimes from one that is affected primarily by changes in fractional vegetation cover to an asymptotic one can be simulated by varying fractional vegetation cover while keeping LAI fixed at a value of about 3 in the vegetated fraction.

The importance of this finding, which by itself is not very startling, is that the identification of the NDVI threshold between a full and a partial vegetation cover allows one to scale NDVI between bare soil and 100% vegetation cover, for which there is a simple square root relation with fractional vegetation cover [Eq. (3)]. Moreover, our calculations suggest that this relation holds equally well for NDVI corrected or uncorrected for atmospheric attenuation. The latter is of practical significance in view of the seeming importance of fractional vegetation cover, which may be more easily obtainable from satellite measurements than is LAI, and the difficulty in accurately correcting for atmospheric attenuation. Scaling not only minimizes the importance of choosing the initial conditions when using land surface model to obtain the surface energy fluxes and soil water content (Gillies et al., 1997), but also may eliminate the need to accurately correct the satellite radiances for atmospheric attenuation. Furthermore, we suggest that fractional vegetation cover, not LAI, is the key variable in determining surface energy fluxes over partial vegetation cover. Indeed, varying both fractional vegetation cover and LAI in a land surface model may be somewhat redundant when the vegetation cover is less than 100%.

Identification of this full-cover value of NDVI (referred to here as $NDVI_s$) may not be straightforward unless the image contains a full range of vegetation cover. In this case, our calculations suggest that the likely value of NDVI will be about 0.05 below the largest values of NDVI. In any case, a reasonable estimate of $NDVI_s$ based on a qualitative inspection of a histogram will likely leave an uncertainty of about ± 0.05 in choosing $NDVI_s$. For a range of NDVI from 0.0 to 0.6, an error of 0.05 would correspond to an error of less than 0.1 in Fr. This still leaves some uncertainty in choosing the bare soil value of NDVI, however.

APPENDIX

The following mathematical development refers to Figure 1, which depicts streams of radiant fluxes above a partial vegetation cover. All fluxes move either upward or downward with respect to a horizontal surface. The fluxes are distributed as follows. A pencil beam of sun-

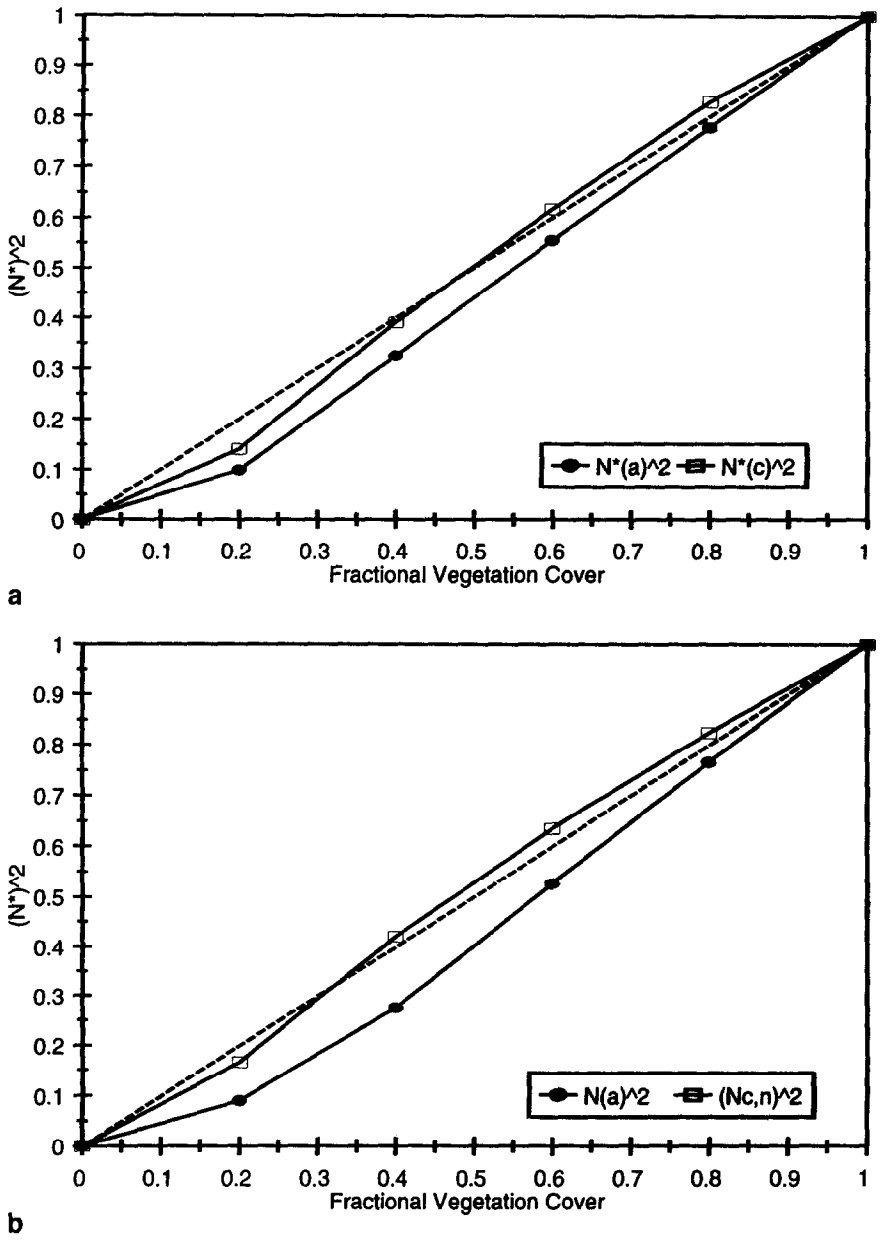

Figure 5. Scaled NDVI squared (N^{*2}) versus fractional vegetation cover based on the apparent [uncorrected, N^* (a); solid circles] and corrected radiances [N^* (c); open rectangles] for a threshold LAI of 3. The dashed line indicates the 1:1 correspondence; (a) 15-km visibility; (b) 5-km visibility.

light (solar constant S_0 adjusted for solar distance) at solar elevation angle φ_0 passes through the atmosphere. The direct flux reaching the surface just above the bare soil and vegetation canopy (F_d) is

$$F_d = S_0 \sin\varphi_0 T_{ab} T_s. \quad \text{(A1.1)}$$

The symbol T represents a broad-band transmittance, defined in general terms as

$$T = e^{-\tau m}, \quad \text{(A1.2)}$$

where τ is a normalized optical depth for that band and m is a path length. T_{ab} and T_s refer to absorption by the direct beam (water vapor, carbon dioxide, ozone, and aerosols) and forward scattering (by air and aerosols), respectively.

Unlike Beer's Law, which it resembles [Eq. (A1.2)], the transmittances refer to a broad-band radiant flux, either diffuse or direct and in the visible or near IR. By definition, the remainder of the incident flux transmitting through a medium $(1-T)$ is split between an absorptance and a reflectance, R. The latter is subdivided into a forward-scattering component and a backward-scattering component, which refer to the fraction of the incident beam scattered upward or downward.

The diffuse flux reaching the surface (F_{df}) is

$$F_{df} = S_0 \sin\varphi_0 [T_{ab}(1-T_s)(1-T_{bs})], \quad \text{(A2)}$$

where T_{bs} refers to the backscattering component of the transmittance. Some of the flux incident on the bare soil surface is reflected back and forth between the atmosphere and soil. If absorption by these multiple reflections and other second-order effects are ignored, the to-

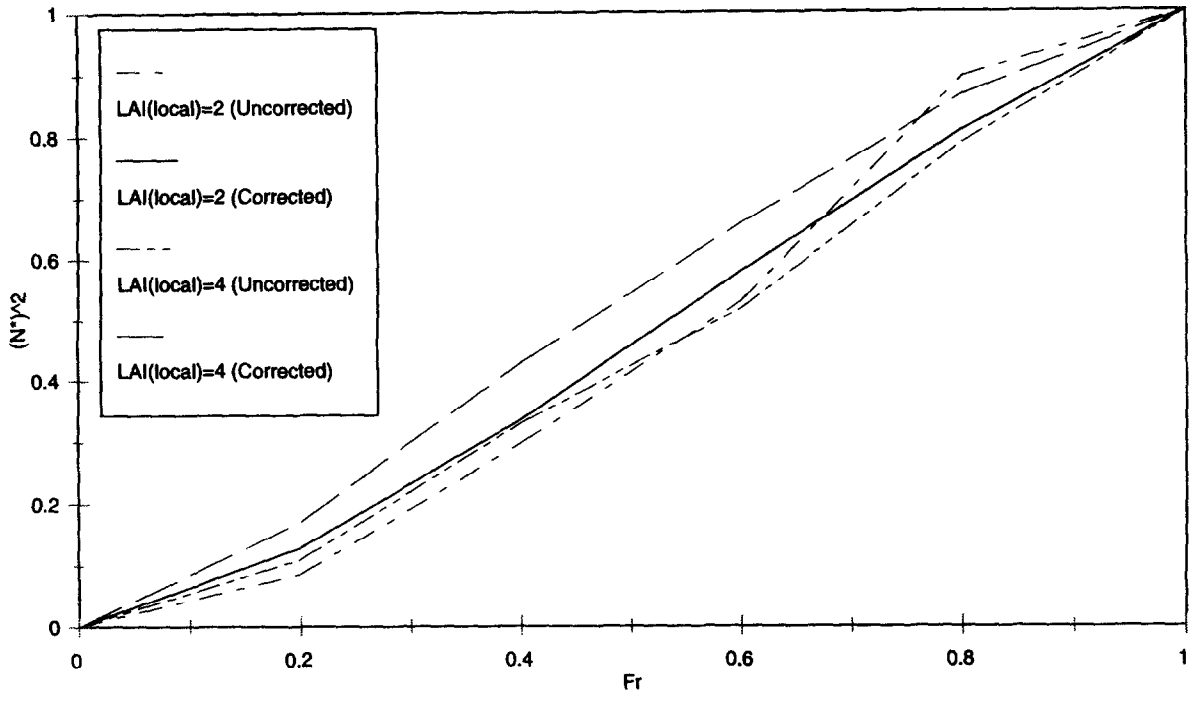

Figure 6. Same as Figure 5a (15-km visibility) but for simulations with threshold values of LAI equal to 2 and 4, for both apparent (uncorrected) $N°$ and corrected radiances. (The 1:1 line is omitted.)

tal direct plus diffuse flux absorbed at the surface in the bare soil portion (F_g) is

$$F_g=\frac{F_d+F_{df}}{1-X}(1-a_g), \qquad \text{(A3.1)}$$

where a_g is the bare soil albedo (identical for direct and diffuse flux) and X is the correction for the internal reflections:

$$X=a_g T_{bsd}(1-T_{scd})T_{abd}\sin\varphi_0. \qquad \text{(A3.2)}$$

T_{bsd}, T_{scd}, and T_{abd} respectively refer to transmittance components for backward scattering of diffuse flux by air and aerosols, forward scattering of diffuse flux, and the absorption of diffuse flux. (Mathematical definitions for the transmittances and the method of calculating them are presented later.) The value of X tends to be very small—about 1 or 2% of the incident flux at the surface.

The flux reflected at the surface over the bare soil (F_{gr}) is approximately

$$F_{gr}=(F_d+F_{df})a_g. \qquad \text{(A3.3)}$$

Both direct (F_d) and diffuse (F_{df}) flux components are also incident at the top of the vegetation canopy. In accord with Taconet et al. (1986), the direct flux penetrating the plant canopy and absorbed at the ground beneath the vegetation (F_{gcd}) is

$$F_{gcd}=F_d[(1-\sigma_f)(1-a_g)/(1-\sigma_f a_g a_f)], \qquad \text{(A4)}$$

where a_g and a_f refer to the albedo of the ground surface and the vegetation, respectively.

The light attenuation factor (canopy transittance) for direct solar flux (σ_f) is calculated by using the formula

$$\sigma_f=e^{-\kappa L/\sin\varphi_0}, \qquad \text{(A5)}$$

where κ is assigned a value for isotropic leaf orientation of 0.4. For the diffuse flux component (F_{gcd}), the diffuse solar angle (φ_0) direction is assigned a value of 54 degrees (path length 1.7). Calculation of the diffuse flux absorbed at the ground beneath the canopy (F_{gcd}) is identical with that of F_{gcd} in Eq. (A4) but with F_{df} replacing F_d and with a canopy transmittance factor (σ_f) for diffuse light ($\sin\varphi_0=1/1.7$).

The direct flux absorbed by the plant canopy (F_{cd}) is

$$F_{cd}=F_d(1-a_f)\sigma_f(1+a_g(1-\sigma_f)/(1-\sigma_f a_g a_f). \qquad \text{(A6.1)}$$

The diffuse flux absorbed by the canopy (F_{cdf}) is similarly calculated but with incident diffuse flux (F_{df}) replacing the incident direct flux (F_d) on top of the canopy and the diffuse path length in σ_f.

The total flux absorbed at the ground under the canopy (F_{gc}) is therefore the sum of F_{gcd} and F_{gc}, and the total flux absorbed in the canopy (F_{can}) is the sum of the diffuse and direct flux components absorbed in the canopy ($F_{cd}+F_{cdf}$). The total flux absorbed in and below the plant canopy (F_c) is the sum of F_{can} and F_{gc}.

Weighted for the fraction of vegetation cover (Fr), the absorbed flux at the surface over both vegetated and bare soil fractions (F_{sab}) is

$$F_{sab}=FrF_c+(1-Fr)F_g. \qquad \text{(A6.2)}$$

The total reflected flux from the canopy (F_{cr}) is not calculated directly. Instead, it is assumed to be the dif-

ference between the incident flux at the top of the canopy and that absorbed in and below the canopy:

$$F_{cr}=F_d+F_{df}-F_c. \tag{A7.1}$$

The total reflected flux over the canopy and bare soil weighted for vegetation cover (F_r) is

$$F_r=FrF_{cr}+(1-Fr)F_{gr}. \tag{A7.2}$$

The reflectivity of that surface (R_{sfc}) is

$$R_{sfc}=\frac{F_r}{(F_d+F_{df})}. \tag{A8}$$

The upwelling solar flux at the top of the atmosphere (F_{out}) is calculated indirectly. It is assumed to be the difference between the incoming solar flux and all the flux components absorbed in the atmosphere and at the surface.

$$F_{out}=S_0\sin\varphi_0-F_{ab}-F_{abr}-F_{sab}. \tag{A9}$$

Here, $F_{ab}=[S_0\sin\varphi_0(1-T_{ab})]$ is the absorbed flux from the downwelling direct beam, F_{abr} is the absorbed flux from the upwelling diffuse radiation stream reflected by the canopy and bare soil surfaces (F_r), and F_{sab} is the total absorbed flux at the surface.

The reflectivity at the top of the atmosphere (R_{top}) is then

$$R_{top}=\frac{F_{out}}{S_0\sin\varphi_0}, \tag{A10}$$

which is to be compared with that at the ground, as expressed by Eq. (A8). Equation (A10) is the at-sensor (apparent) reflectivity measured by satellite, whereas Eq. (A8) is considered to be "corrected" reflectivity that is independent of the intervening atmosphere.

Transmittances are calculated separately for scattering and absorption. For Rayleigh scattering by air molecules, the normalized optical depth τ_R is expressed as

$$\tau_R=0.0088\lambda^{x(\lambda)}, \tag{A11.1}$$

where $x(\lambda)$, a function of wavelength λ (in micrometers), is equal to $(-4.15+0.2\lambda)P_s/1013$, where P_s is the surface pressure in millibars. Path length, m [see Eq. (A1.2)] is computed from the equation

$$1/m=\sin\varphi_0+0.15(\varphi_0+3.88)^{-1.253}. \tag{A11.2}$$

Then the transmittance for Rayleigh scattering (T_R) is

$$T_R=\frac{1}{S_0\Delta\lambda}\int_{\lambda_1}^{\lambda_2}S_{0\lambda}[e^{(-\tau_R m)}]d\lambda, \tag{A11.3}$$

where φ_0 is taken in degrees, $\Delta\lambda$ is the radiation band width in micrometers pertaining to the limits of the integral, and $S_{0\lambda}$ is the extraterrestrial solar flux as a function of wavelength. S_0 represents the integrated flux in the band. The integral therefore represents a weighted mean transmittance over the wavelength band, λ=0.5–0.7 μm (visible band) and λ=0.7–0.9 μm (near IR band).

Transmittance for atmospheric aerosols (T_D) is calculated in a similar manner.

$$T_D=\frac{1}{S_0\Delta\lambda}\int_{\lambda_1}^{\lambda_2}S_{0\lambda}[e^{(-\tau_D m)}]d\lambda, \tag{A12.1}$$

where τ_D is the normalized optical depth for aerosols (dust). In accord with Paltridge and Platt, we write the Angstrom turbidity law:

$$\tau=\beta\lambda^{-a}, \tag{A12.2}$$

where β is the Angstrom turbidity coefficient and the exponent a depends on the type of aerosol; a value of 1.0 was chosen for a, which is typical for natural continental aerosols. Coefficient β is related to the aerosol optical depth at 0.5 μm through Eq. (12.2):

$$\beta=\tau_D(\lambda=0.5\mu m)/(0.5^{-a}), \tag{A12.3}$$

where $\tau_D(\lambda=0.5\ \mu\text{m})$ is determined from the horizontal visibility (V; km) as

$$\tau_D(\lambda=0.5\mu m)=3.91/V. \tag{A12.4}$$

Thus aerosol transmittance is varied as a function of the aerosol optical depth at 0.5 μm as indicated by the horizontal visibility. We divide τ_D into two components, one for scattering (τ_s) and one for absorption (τ_A), where $\tau_s=0.75\tau_D$ and $\tau_A=0.25\tau_D$, which yield the transmittances for scaterring and absorption by dust, respectively T_{Ds} and T_{Da}. Then the scattering transmittance (T_s) is calculated as the product of scattering transmittances.

$$T_s=T_RT_{Ds}. \tag{A13.1}$$

Absorption of radiation by water vapor, carbon dioxide, and oxygen is neglected, because these effects are assumed to be small—between 0.5 and 0.9 μm, although a weak water vapor band exists near 0.74 μm and there is a very weak oxygen band at 0.68 μm. A small correction is made for ozone (normalized depth 0.3 cm) in the Chappuis (visible) band by using a method outlined by Paltridge and Platt (1976); see Lacis and Hansen (1974). This correction will not be discussed except to indicate that T_{oz} is computed only for the visible band and its numerical value is very nearly equal to 1.0.

The only significant absorber therefore in either the visible or the near IR band is aerosol. Thus,

$$T_{ab}=T_{oz}T_{Da}. \tag{A13.2}$$

In calculating the diffuse transmittance functions in Eq. (A3.2), we calculate T_{sod} and T_{abd} in a manner identical with that for T_s and T_{ab}, except that a solar angle of 54 degrees is used for the equivalent solar angle of diffuse isotropic solar radiation.

For backscattered flux (F_{bs}), which does not reach the surface, the transmittance (T_{bs}) is calculated by assuming that half of the Raleigh scattering by air molecules is directed backward (toward the top of the atmosphere) and half downward. For dust, we assume that

Table 2. Values of Parameters Used in Simulations

Parameter (Units)	*Value*
Time (LST)	1300
Day	7
Month	July
Latitude (deg)	40.7
Longitude (deg)	76.6
Satellite nadir angle (deg)	10
Visibility (km)	10, 5
Precipitable water (cm)	1.5
Surface pressure (mb)	1000
Canopy extinction coefficient	0.4
Fraction veg cover*	0.6
LAI (local)*	3
a (visible; satellite)*	0.12
a (visible; surface)*	0.07
a (near IR; satellite)*	0.32
a (near IR; surface)*	0.36

* Values of parameters specific to a single example for case with 15-km visibility.

the fraction backscattered is only 0.2, leaving 0.8 of the scattered flux directed toward the ground. Therefore, the bulk backscattering transmittance for dust and air is

$$T_{bs}=[0.5(1-T_r)+(0.2+0.3\cos\varphi_0)(1-T_{Ds})]/[(1-T_{Ds})+(1-T_R)], \quad \text{(A14.1)}$$

where the cosine function accounts for the highly anisotropic nature of aerosol scattering in which increasing amounts of scattering occur in the upward direction as the solar elevation angle decreases from solar noon (20% of the scattered flux directed upward) to near the horizon (50% directed downward).

Values of parameters used to perform the simulations from which the illustrations in this article were obtained are given in Table 2.

We would like to thank Professor John Norman, for his comments on the paper, and our sponsor, the USDA, under cooperative agreement No. 58-1270-3-030.

REFERENCES

Asrar, G., Fuchs, M., Kanemasu, E. T., and Hatfield, J. L. (1984), Estimating absorbed photosynthetic radiation and leaf area index from spectral reflectance in wheat. *Agron. J.* 76:300–306.

Best, E. G., and Harlan, J. C. (1985), Spectral estimation of green leaf area index of oats. *Remote Sens. Environ.* 17: 27–36.

Carlson, T. N., Perry, E. M., and Schmugge, T. J. (1990), Remote estimation of soil moisture availability and fractional vegetation cover for agricultural fields. *Agric. For. Meteorol.* 52:45–69.

Choudhury, B. J., Ahmed, N. U., Idso, S. B., Reginato, R. J., and Daughtry, C. S. T. (1994), Relations between evaporation coefficients and vegetation indices studied by model simulations. *Remote Sens. Environ.* 50:1–17.

Curran, P. J. (1983), Multispectral remote sensing for the estimation of green leaf area index. *Philos. Trans. R. Lond. Ser. A* 309:257–270.

Dickinson, R. E., Henderson-Sellers, A., and Kennedy, P. J. (1993), Biosphere-atmosphere transfer scheme (BATS) version 1e as coupled to the NCAR community climate model. *NCAR Tech. Note NCAR/TN-387+STR, NCAR*, Boulder, CO.

Gallo, T. F., Daughtry, C. S. T., and Bauer, M. E. (1985), Spectral estimation of absorbed photosynthically active radiation in corn canopies. *Remote Sens. Environ.* 17:221–232.

Gillies, R. R., Cui, J., Carlson, T. N., Kustas, W. P., and Humes, K. S. (1997), Verification of a method for obtaining surface soil water content and energy fluxes from remote measurements of NDVI and surface radiant temperature. *Int. J. Remote Sens.* (in press).

Gillies, R. R., and Carlson, T. N. (1995), Thermal remote sensing of surface soil water content with partial vegetation cover for incorporation into climate models. *J. Appl. Meteorol.* 34:745–756.

Holben, B. N., Tucker, C. J. and Fan, C. J. (1980), Spectral assessment of soybean leaf area and leaf biomass. *Photogramm. Eng.* 45:651–656.

Jasinski, M. F. (1996), Estimation of subpixel vegetation density of natural regions using satellite multispectral imagery. *IEEE Trans. Geosci. Remote Sens.* 34:804–813.

Kneizys, F. X., Abreu, L. W., Anderson, G. P., Chetwynd, J. H., Shettle, E. P., Berk, A., Bernstein, L. S., Robertson, D. C., Acharya, P., Rothman, L. S., Selby, J. E. A., Gallery, W. O., and Clough, S. A. (1996), *The MODTRAN 2/3 Report and LOWTRAN 7 Model* (L. W. Abreu and G. P. Anderson, Eds.), prepared by Ontar Corp., North Andover, MA, for Phillips Laboratory, Geophysical Directorate, Hanscom AFB, MA., Contract No. F19628-91-C-0132.

Kneizys, F. X., Shettle, E. P., Abreu, L. W., Cheytwynd, J. H., Anderson, G. P., Gallery, W. O., Selby, J. E., and Clough, S. A. (1988), *Users Guide to Lowtran-7*, Air Force Geophysics Laboratory Research Paper No. 401010, Project No. 7670.

Lacis, A. A., and Hansen, J. E. (1974), A parameterization for the absorption of solar radiation in the earth's atmosphere. *J. Atmos. Sci.* 31:118–133.

Leprieur, C., Kerr, Y. H., and Pichon, J. M. (1996), Critical assessment of vegetation indices from AVHRR in a semi-arid environment. *Int. J. Remote Sens.* 17:2594–2563.

Liu, Q., and Huete, A. (1995), A feedback based modification of the NDVI to minimize canopy background and atmospheric noise. *IEEE Trans. Geosci. Remote Sens.* 33:457–465.

Monteith, J. L. (1973), *Principles of Environmental Physics*. Arnold, p. 197.

Nemani, R., and Running, S. W. (1989), Testing a theoretical climate-soil-leaf area hydrological equilibrium of forests using satellite data and ecosystem simulation. *Agric. For. Meteorol.* 44:245–260.

Olioso, A., Carlson, T. N., and Brisson, N. (1995), Simulation of diurnal transpiration and photosynthesis of a water stressed soybean crop. *Agric. For. Meteorol.* 81:41–59.

Paltridge, G. and Barber, J. (1988), Monitoring grassland dryness and fire potential in Australia with NOAA/AVHRR data. *Remote Sens. Environ.* 28:384–393.

Paltridge. G. W., and Platt, C. M. R. (1976), *Radiative Processes in Meteorology and Climatology*. Elsevier, Amsterdam.

Pinty, B., and Verstraete, H. M. (1992), "GEMI": a non-linear index to monitor global vegetation from satellites. *Vegetation* 101:15–20.

Pollard, D., and Thompson, S. (1995), Use of land-surface transfer schemer (LSX) in a global climate model: the response to doubling stomatal resistance. *Global Planet. Change* 10:130–161.

Price, J. C. (1992), Estimating vegetation amount from visible and near infrared reflectances. *Remote Sens. Environ.* 41: 29–34.

Sellers, P. J. (1985), Canopy reflectance, photosynthesis and transpiration. *Int. J. of Remote Sens.* 10:855–867.

Sellers, P. J., and Dorman, J. L. (1987), Testing the simple biosphere model (SiB) using point micrometeorological and biophysical data. *J. Clim. Appl. Meteorol.* 26:622–651.

Tucker, C. J. (1979), Red and photographic infrared linear combinations for monitoring vegetation. *Remote Sens. Environ.* 8:127–150.

Taconet, O., Carlson T. N., Bernard, R., Vidal-Madjar, D. (1986), Evaluation of a surface/vegetation model using satellite infrared surface temperatures. *J. Clim. Appl. Meteorol.* 25:1752–1767.

Wetzel, P. J., and Boone, A. (1995), A parameterization for land-atmosphere-cloud exchange (PLACE): documentation and testing of a detailed process model of the partly cloudy boundary layer over heterogeneous land. *J. Clim.* 8: 1810–1837.